# III-V Heterostructure Grown on 300mm Ge/Si Wafer for Large-Scale Fabrication of Red $\mu$-LEDs

P. Gaillard, A. Ndiaye, B. Ben Bakir, P. Le Maitre, J. Da Fonseca, J. M. Hartmann, M. Martin, J. Moeyaert, H. Mehdi, T. Baron, and C. Jany

***Abstract*— We report on the design, fabrication and characterization of red $\mu$-LEDs directly grown on large-scale silicon wafers through a superior-quality Ge buffer. 300mm Ge/Si substrates with a threading dislocation density (TDD) of $\sim 10^7$ cm$^{-2}$ were successfully achieved, then followed by the growth and process of visible 649nm AlGaAs-based red emitters. The electro-optical properties of various red $\mu$-LEDs with diameters ranging from 10 to 100$\mu$m are investigated, showing promising performances. Those results coupled with numerical analysis with a model based on transfer-matrix with dipole source-terms help us better identify the main challenges limiting the efficiencies of our devices, while providing optimization routes to alleviate them. We believe that these results could pave the way for a monolithic large-scale and low-cost integration of red $\mu$-LEDs on 300mm Si-CMOS driving circuits and for the fabrication of high-resolution RGB microdisplays that see use in various applications in optoelectronics.**

***Index Terms*— Red $\mu$-LEDs, direct epitaxy, AlGaAs, silicon, 300 mm, low TDD, Ge on Si.**

## I. Introduction

MICROSIZED inorganic light-emitting diodes ($\mu$-LEDs) have been foreseen as the next-generation display technology for various applications in the field of optoelectronics, e.g., optical communication, wearables and most recently augmented-reality devices due to their self-emissive nature, their high resolution and longer lifetime compared to other existing technologies [1]. For large-scale full-color applications, one needs to efficiently and monolithically integrate at least three primary colors (Red, Green and Blue) per pixel on single 8" to 12" silicon substrates, which are the basis of Si-CMOS driving circuits.

So far, state-of-the-art blue and green $\mu$-LEDs mainly rely on $In_xGa_{1-x}N$ alloys, which could theoretically span the entire visible spectrum by varying their Indium composition. Despite the exciting performances already achieved, their efficiencies start to decrease abruptly in the red spectral range ($x \geq 40\%$) due to the important lattice mismatch between InGaN and GaN leading to a poor crystal quality as well as a decrease of the radiative recombination efficiency stemming from an increased quantum Stark effect (QCSE) [2]. Hence, arsenide- and phosphide-based material systems have been the best candidates for red LEDs up to now [3].

Integrating such semiconductors on Si wafers can however be very tricky. While the standard transfer techniques based on the pick-and-place method are failing to meet the industrial demands in terms of reliability, direct epitaxy is gaining a lot of ground as a suitable technique [4]. Indeed, notwithstanding the wealth of recent developments in epitaxy of InGaN blue and green $\mu$-LEDs on Si substrates [5], the direct growth of red $\mu$-LEDs on the same wafer remains a challenge. In fact, those epilayers are grown lattice-matched on 2" to 4" GaAs substrates. Due to the large lattice mismatch between Si and GaAs (4.1%), a direct growth of those epilayers on large-scale Si wafers leads to a high threading dislocation density (TDD), which decreases the brightness of the resulting devices [6]. Recent works however suggest that they are different routes to alleviate this issue [7], [8], among which the use of Ge layer, which we will focus in this work [9]. However, to the best of our knowledge, this has not been achieved yet on large-scale 300mm silicon wafers.

This work deals with the demonstration of red $\mu$-LEDs directly grown on 300mm silicon wafers thanks to Ge strain-relaxed buffers. The growth and process details are outlined in section II, while in section III the electro-optical properties of the fabricated red $\mu$-LEDs (from 10$\mu$m- to 100$\mu$m-sized) are investigated. Those analyses help us provide different optimization routes and guidelines that could pave the way for the monolithic large-scale and low-cost integration of red $\mu$-LEDs on 300mm Si-CMOS driving circuits and the fabrication of high-resolution RGB microdisplays.

## II. Materials and Fabrication Details

Following the same growth procedure as in [10] and [11], we obtain a superior quality Ge buffer layer with state-of-the art characteristics [9]: a roughness of $\sim$0.8nm quantified by atomic force microscopy (AFM) as well as a TDD of $\sim 10^7$ cm$^{-2}$ evaluated by electron channeling contrast imagery (ECCI). Subsequently, the AlGaAs-based heterostructure, designed to reach its peak emission wavelength at $\sim$650nm, is grown on the so-formed Ge/Si 300mm wafer in an Applied Materials MOCVD 300 mm cluster tool. Prior to the growth, a SiCoNi$^{TM}$ treatment is performed on the Ge/Si to remove any oxide present on its surface. Trimethylgallium

Manuscript received 19 October 2022; revised 11 November 2022; accepted 25 November 2022. Date of publication 28 November 2022; date of current version 7 December 2022. This work was supported in part by the French Recherches Technologiques de Base (Basis Technologies Research), RENATECH Programs and the French National Research Agency in the framework of the Investissements d'Avenir Program under Grant ANR-10-IRT-05 and Grant ANR-15-IDEX-02. *(Corresponding author: C. Jany.)*

P. Gaillard, A. Ndiaye, B. Ben Bakir, P. Le Maitre, J. Da Fonseca, J. M. Hartmann, and C. Jany are with LETI, CEA, MINATEC Campus, 38054 Grenoble, France (e-mail: christophe.jany@cea.fr).

M. Martin, J. Moeyaert, H. Mehdi, and T. Baron are with CNRS, CEA/LETI Minatec, LTM, Université Grenoble Alpes, 38054 Grenoble, France (e-mail: thierry.baron@cea.fr).

Digital Object Identifier 10.1109/LPT.2022.3225219

TABLE I
EITAXIAL GROWTH LAYER STRUCTURE AND CHARACTERITICS

| Layer | Material | Thickness (nm) | Doping | TDDs ($cm^{-2}$) |
|---|---|---|---|---|
| **P contact** | GaAs | 115 | Zn ($5.10^{19}$ $cm^{-3}$) | $10^7$ |
| | $Al_{0.45}Ga_{0.55}As$ | 500 | Zn($4.10^{17}$ $cm^{-3}$) | $10^7$ |
| **NID SCH** | $Al_{0.45}Ga_{0.55}As$ | 40 | - | $10^7$ |
| **NID Barrier** | 6 x $Al_{0.45}Ga_{0.55}As$ | 10 | - | $10^7$ |
| **NID QWs** | 6 x $Al_{0.3}Ga_{0.7}As$ | 3 | - | $10^7$ |
| **NID SCH** | $Al_{0.45}Ga_{0.55}As$ | 50 | - | $10^7$ |
| **N Cladding** | $Al_{0.45}Ga_{0.55}As$ | 500 | Si($7.10^{17}$ $cm^{-3}$) | $10^7$ |
| **N contact** | GaAs | 500 | Si($6.10^{18}$ $cm^{-3}$) | $10^7$ |
| **N-Buffer** | Ge | 500 | P($4.10^{19}$ $cm^{-3}$) | $10^7$ |
| **Buffer** | Ge | 1000 | - | $10^7$ |
| **Substrate** | Si | - | - | - |

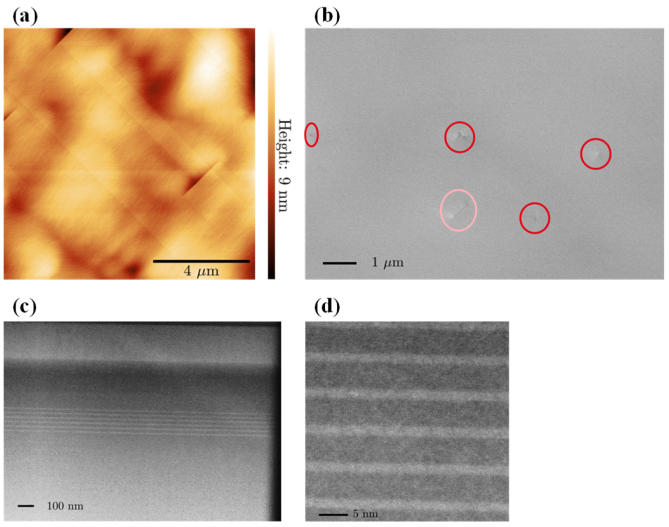


Fig. 1. (a) AFM and b) ECCI-SEM images of entire the epilayer stack at the center and edge, respectively. (c) and (d) HAADF-TEM images of the quantum wells.

(TMGa), trimethylaluminium (TMAl) and tertiarybutylarsine (TBAs) are then used as precursors for Ga, Al and As, respectively, along with $H_2$ as a carrier gas. On the other hand, diethylzinc (DEZ) and silane are used respectively for P et N doping.

Table I summarizes the obtained PIN diode structure. Let us note that a 500nm-thick part of the Ge buffer is N-doped (see Table I) to ensure a good doping level for the GaAs N-contact layer.

The morphological characteristics (AFM, ECCI and HAADF-TEM) of the full stack are shown in Fig. 1.

The roughness (see Fig. 1 (a)) is around 1.2nm while the TDD has the same value as the one measured on the Ge buffer layer (see Fig. 1 (b)). Similar AFM and ECCI measurements are performed at different positions on the wafer showing good uniformity. In addition, a QW width of 3nm is measured from the high-angle annular dark-field (HAADF) transmission electron microscope (TEM) images, which is in agreement with the expected value.

After the epitaxial growth, the 300mm wafer is downsized into 100mm wafers for device fabrication which relies on a vertical integration of circular $\mu$-LEDs with diameters ranging

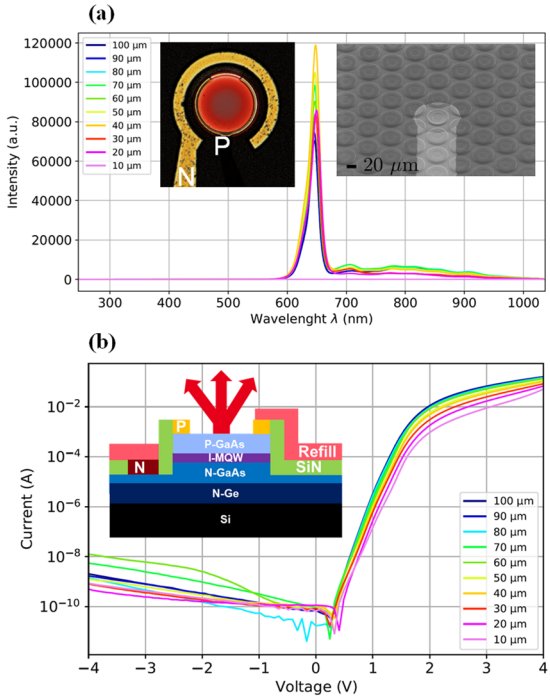


Fig. 2. (a) Electroluminescence spectra and (b) current-voltage characteristics for $\mu$-LEDs with diameters ranging from 10$\mu$m to 100$\mu$m. Top and cross views of the device structure are displayed in the inset, as well 15$\mu$m-thick $\mu$-LED array.

from 10 to 100$\mu$m. The process starts with the deposition of Ti/Pt as a P-type contact in a ring-like geometry by e-beam evaporation. The definition of the mesa structure then ensues with successive deposition of a SiN/ $SiO_2$bilayer hard mask (HM) by plasma-enhanced chemical vapor deposition (PECVD). After a photo-lithography step, the bi-layer HM is subsequently etched by $CHF_3$and $SF_6$-based induced coupled plasma (ICP). Thereafter, the III-V heterostructure is etched down to the N-GaAs layer with a $SiCl_4$/Ar-based plasma. The remaining HM is removed by dry etching. Next, the devices are passivated by a PECVD-SiN layer, which is later on etched with $SF_6$-based ICP. This through passivation opening allows for the Ni/Ge/Au N-contact deposition by e-beam evaporation. The process flow finishes with a Ti/Au-based reload deposition for both contacts in the PECVD chamber and an annealing at 395°C. Different chips of a 100mm wafer were characterized to perform statistical analyses and evaluate process repeatability.

## III. RESULTS AND DISCUSSION

Fig. 2 (a) shows the electroluminescence (EL) spectra for the different $\mu$-LED sizes with similar Lorentzian shapes (emission peak at ∼649nm and full widths at half maximum (FWHM) of ∼24nm, which are in close agreement with the simulations. We can also notice that the peak intensity is $\mu$-LED-size dependent: the highest and lowest intensities are obtained for the 40$\mu$m-sized and 100$\mu$m-sized $\mu$-LEDs, respectively.

Fig. 2 (b) depicts the current-voltage (I-V) characteristics of the fabricated $\mu$-LEDs. The current at 4V is decreasing with the $\mu$-LED size meaning there is a higher resistance in the

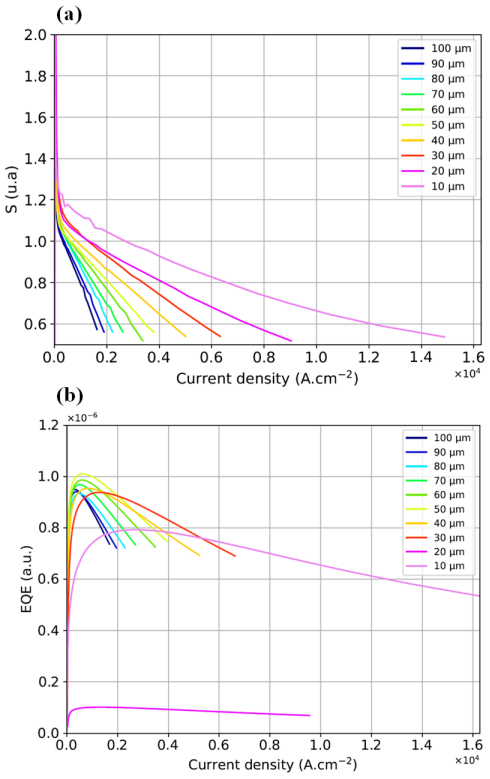


Fig. 3. S-parameter and (b) EQE as a function of current density for $\mu$-LEDs with diameters ranging from 10$\mu$m to 100$\mu$m.

smaller $\mu$LEDs as explained in [12]. It is also seen that the I-V curves are highly dependent on the size of the $\mu$-LEDs.

Several parameters can be extracted from these I-V curves to better our understanding of their shapes. First, we evaluate the ideality factor, $n_{ideal}$, which enables the identification of the recombination mechanisms at play here [13]. From the I-V characteristics, we find low-injection-current values of $n_{ideal}$ between 3.42 and 2.49 for 10$\mu$m-sized and 100$\mu$m-sized $\mu$-LEDs, respectively, suggesting that defect-assisted carrier tunneling occurs in our devices [13]. In addition, the saturation current is found to have very low values between 0.65pA and 2.4pA, which can be attributed to two possible phenomena: a low leakage current because of a high doping level in the epilayers or the fact that a large part of the leakage current is caught by the aforementioned defects. We can finally emphasize that the series resistance ($R_S$) is also extracted from the I-V curves and varies from 18 to 10$\Omega$ with decreasing $\mu$-LED diameters [12], which is consistent with the size-dependency of the I-V curves mentioned above.

To analyze our results further, we report on the S-parameter and the external quantum efficiency (EQE) as a function of current density in Fig. 3, which are derived from current-voltage-luminance (IVL) measurements. As $n_{ideal}$, S-parameter also describes the different recombination mechanisms [13], albeit as a function of the current density, facilitating the understanding of the different regimes and analysis the EQE values in Fig. 3 b). In the Fig 3(a), we can first observe that at very low current densities, S-parameter has a value of 2 corresponding to non-radiative Shockley-Read-Hall (SRH) recombinations due to defects, which is in close agreement with the values of the $n_{ideal}$ and the TDD values. Subsequently, until 2.10$^3$ A.cm$^{-2}$, the S-parameter values decrease to 1, which is the signature of band-to-band radiative recombinations. The last regime denotes the carrier-leakage through overflow that occurs at high current densities in the quantum wells, where the Fermi level rises to the top of the barriers. The active region is then so flooded with carriers that even when increasing current-injection densities, the carrier concentration is saturated [14]. We can highlight that the radiative-recombination regime is very small compared to the leakage one, which is a very common behavior in high-mobility III-V materials [15].

The EQE variations as a function of the current density are shown in Fig. 3 (b). As expected, EQE is strongly $\mu$-LED-size dependent. Particularly, larger $\mu$-LEDs reach their peak EQE at lower current densities than smaller ones (e.g., at 360 A/cm$^2$ and 562.5 A/cm$^2$ for 100$\mu$m- and 60$\mu$m-sized devices, respectively), which is due to an increase of non-radiative recombinations for decreasing $\mu$-LED sizes [16]. The highest EQE values of $\sim$10$^{-6}$ are achieved for 50$\mu$m-sized $\mu$-LEDs. We can also note that the drop after the EQE maxima occurs faster in terms of current density for 100$\mu$m-sized devices than 20$\mu$m ones, which can be attributed to a better spreading in smaller $\mu$-LED since less area is to be covered by the injected current [17]. Moreover, the aforementioned EQE variations could be directly related to the S-parameters displayed in Fig. 3 (a). In fact, the EQE reaches its maximum values at current densities matching the radiative regime spotted by the S-parameters above, while it starts to drop in regions where carrier-leakage through overflow occurs in the quantum wells. Additional statistical analyses performed on $\mu$-LED arrays on different chips showed a uniformity of the electro-optical properties in the IVL curves (standard deviation less than 5%).

Since this demonstration is the first technological run of red $\mu$-LEDs on 300mm Ge/Si wafers, our EQE values are 4 orders of magnitude below the ones of state-of-the-art red $\mu$-LEDs on lower-scale wafers as in [15], [16], and [17].

To explore how better epitaxial design could help overcome this EQE limit, we performed additional numerical simulations using a well-established transfer-matrix method with dipole source terms [18]. From these simulations, we are able to analyze spontaneous emission distribution inside the epilayer structures as well as light extraction mechanisms. We find that the light extraction efficiency (LEE) of our red $\mu$-LEDs is limited to less than 1%, because a large part of the emitted light is guided inside the multilayer structure. $\sim$35% of this non-outcoupled light is pseudo-guided in the whole epilayer structure and will eventually be absorbed by the N-GaAs or the Ge layer, while $\sim$63% of it couple to the available guided modes inside the Ge layer ($>$15 modes). Since the Ge buffer behaves as a highly absorbing waveguide in the red spectral range, all this light will also eventually be lost in the Ge layer. From this modal analysis, it appears that LEE strongly limits the EQE of our red $\mu$-LEDs and the main limitations stem from the high-refractive index and absorbing Ge buffer layer ($\sim$63% of the emitted light). They are thus numerous levers in our epitaxial design that could help us improve our LEE

and thus gain at least two orders of magnitude in the EQE of our future structures.

For instance, using AlGaAs/GaAs distributed Bragg reflectors (DBR) on top of the N-type GaAs layer could help circumvent the light loss in the Ge layer, since most of the bottom emitted light would be redirected towards the top of the device. Given that, by thinning the remaining layers and particularly etching the top absorbing P-GaAs, a thinner optical cavity would be formed between the DBR and the top side of the $\mu$-LEDs. Since this thinner cavity would support less guided modes in non-absorbing layers, then the two previous strategies could be combined with surface texturing such as photonic-crystals (PhCs). In this framework, LEE above 40% could be expected as well as a better directionality of the emission patterns, which would strongly improve the EQE and the brightness of the devices [19]. Finally yet importantly, we are currently examining the possibility of elaborating these red $\mu$-LEDs with InGaP/AlGaInP quantum wells. Those quaternary alloys are expected to have better internal efficiencies than ternary ones and thus could help limit the defects in the epilayer that are very detrimental to the electro-optical performances of the devices [3].

Despite these limitations, IVL measurements showed us that luminance values as high as $2.10^4$ cd.m$^{-2}$ have been achieved for our red $\mu$-LEDs, which is close to the luminances of state-of-the-art $\mu$-LEDs [12] but at current density 3 order of magnitude lower than for our LEDs. Some improvements would need to be implemented to obtain this level of luminance at lower current density. In that regard, combining all these aforementioned optimization strategies could help alleviate these issues and better integrate red $\mu$-LEDs on large silicon wafers.

## IV. Conclusion

In this letter, we have dealt with the demonstration of red $\mu$-LEDs directly grown on 300mm silicon wafers through a Ge buffer. High-quality 300mm Ge/Si substrates with a TDD of $\sim 10^7$ cm$^{-2}$ were successfully achieved and followed by the growth of visible 649nm AlGaAs-based red devices for the sake of demonstration. The electro-optical properties of various red $\mu$-LEDs with diameters ranging from 10 to 100$\mu$m have been investigated showing that eventually luminance values as high as $2.10^4$ cd.m$^{-2}$ could be achieved along with promising performances. Additional numerical analyses have helped us point out that light loss in the Ge buffer ($\sim$63%) drastically limits the LEE of the devices ($<$1%), which plays a very detrimental role on the overall efficiency of the red $\mu$-LEDs. The issues could be alleviated by optimizing the epitaxial design through the insertion of distributed Bragg reflectors, thinning ofepilayers, surface texturing and the use of quaternary alloys instead of ternary ones. Current and future works are mainly focused on devising strategies to improve the electro-optical performances of those devices throughout all these optimization routes.

We believe that these results on large-area 300mm Si substrates could pave the way for a monolithic large-scale and low-cost integration of red $\mu$-LEDs on 300mm Si-CMOS driving circuits and the fabrication of high-resolution RGB microdisplays that see use in various applications in optoelectronics.

## Acknowledgment

The authors want to thank the CEA Leti Cleanroom Staff, the Nanocharacterization Platform (PFNC) especially E. Gautier for the TEM characterization, as well as Applied Materials for technical assistance on the MOCVD tool and fruitful discussions.

## References

[1] E. Quesnel et al., "Dimensioning a full color LED microdisplay for augmented reality headset in a very bright environment," *J. Soc. Inf. Disp.*, vol. 29, no. 1, pp. 3–16, 2021, doi: 10.1002/jsid.884.

[2] Z. Zhuang, D. Iida, and K. Ohkawa, "Investigation of InGaN-based red/green micro-light-emitting diodes," *Opt. Lett.*, vol. 46, no. 8, pp. 1912–1915, 2021, doi: 10.1364/OL.422579.

[3] K. Streubel, N. Linder, R. Wirth, and A. Jaeger, "High brightness AlGaInP light-emitting diodes," *IEEE J. Sel. Topics Quantum Electron.*, vol. 8, no. 2, pp. 321–332, Mar. 2002, doi: 10.1109/2944.999187.

[4] F. Templier and J. Bernard, "18–3: A new approach for fabricating high-performance MicroLED displays," in *SID Symp. Dig. Tech. Papers*, vol. 50, no. 1, Jun. 2019, pp. 240–243, doi: 10.1002/sdtp.12900.

[5] S.-Y. Nunoue et al., "LED manufacturing issues concerning gallium nitride-on-silicon (GaN-on-Si) technology and wafer scale up challenges," in *IEDM Tech. Dig.*, Dec. 2013, p. 13, doi: 10.1109/IEDM.2013.6724622.

[6] R. Alcotte et al., "Epitaxial growth of antiphase boundary free GaAs layer on 300 mm Si(001) substrate by metalorganic chemical vapour deposition with high mobility," *APL Mater.*, vol. 4, no. 4, Apr. 2016, Art. no. 046101, doi: 10.1063/1.4945586.

[7] C. Shang et al., "High-temperature reliable quantum-dot lasers on Si with misfit and threading dislocation filters," *Optica*, vol. 8, no. 5, pp. 749–754, May 2021, doi: 10.1364/OPTICA.423360.

[8] C. Shang et al., "Electrically pumped quantum-dot lasers grown on 300 mm patterned Si photonic wafers," *Light, Sci. Appl.*, vol. 11, no. 1, Oct. 2022, doi: 10.1038/s41377-022-00982-7.

[9] Y. Wang et al., "Performance of AlGaInP LEDs on silicon substrates through low threading dislocation density (TDD) germanium buffer layer," *Semicond. Sci. Technol.*, vol. 33, no. 10, Sep. 2018, Art. no. 104004, doi: 10.1088/1361-6641/aadc27.

[10] Y. Bogumilowicz et al., "Threading dislocations in GaAs epitaxial layers on various thickness Ge buffers on 300mm Si substrates," *J. Cryst. Growth*, vol. 453, pp. 180–187, Nov. 2016, doi: 10.1016/j.jcrysgro.2016.08.022.

[11] H. Mehdi et al., "Monolithic integration of GaAs p–i–n photodetectors grown on 300 mm silicon wafers," *AIP Adv.*, vol. 10, no. 12, Dec. 2020, Art. no. 125204, doi: 10.1063/5.0030677.

[12] W. Tian and J. Li, "Size-dependent optical-electrical characteristics of blue GaN/InGaN micro-light-emitting diodes," *Appl. Opt.*, vol. 59, no. 29, pp. 9225–9232, Oct. 2020, doi: 10.1364/AO.405572.

[13] A. B. M. H. Islam, T. K. Kim, D.-S. Shin, J.-I. Shim, and J. S. Kwak, "Generation of sidewall defects in InGaN/GaN blue micro-LEDs under forward-current stress," *Appl. Phys. Lett.*, vol. 121, no. 1, Jul. 2022, Art. no. 013501, doi: 10.1063/5.0089650.

[14] E. F. Schubert, *Light-Emitting Diodes*, E. F. Schubert, Ed., 3rd ed. New York, NY, USA: Cambridge Univ. Press, 2018.

[15] C. Wu and E. S. Yang, "Physical mechanisms of carrier leakage in DH injection lasers," *J. Appl. Phys.*, vol. 49, no. 6, pp. 3114–3117, Jun. 1978, doi: 10.1063/1.325302.

[16] P. Tian et al., "Size-dependent efficiency and efficiency droop of blue InGaN micro-light emitting diodes," *Appl. Phys. Lett.*, vol. 101, no. 23, Dec. 2012, Art. no. 231110, doi: 10.1063/1.4769835.

[17] D. Hwang, A. Mughal, C. D. Pynn, S. Nakamura, and S. P. DenBaars, "Sustained high external quantum efficiency in ultrasmall blue III–nitride micro-LEDs," *Appl. Phys. Exp.*, vol. 10, no. 3, Feb. 2017, Art. no. 032101, doi: 10.7567/APEX.10.032101.

[18] H. Benisty, R. Stanley, and M. Mayer, "Method of source terms for dipole emission modification in modes of arbitrary planar structures," *J. Opt. Soc. Amer. A, Opt. Image Sci.*, vol. 15, no. 5, pp. 1192–1201, May 1998, doi: 10.1364/JOSAA.15.001192.

[19] A. Ndiaye, H. S. Nguyen, C. Seassal, E. Drouard, and B. Ben Bakir, "Farfield pattern and guided-mode extraction analysis for highly directional emission from photonic-crystal based AlGaInP/InGaP MQW color-converters in thin-film geometry," *AIP Adv.*, vol. 12, no. 4, Apr. 2022, Art. no. 045122, doi: 10.1063/5.0085930.